International Journal of Heat and Mass Transfer 149 (2020) 119057

Contents lists available at ScienceDirect

International Journal of Heat and Mass Transfer

journal homepage: www.elsevier.com/locate/hmt

Quantitative experimental determination of evaporation influencing factors in single droplet levitation

Malte Junk[a], Jörn Hinrichs[b], Fritz Polt[a], Jonas Fechner[a], Werner Pauer[a,*]

[a] Institute for Technical and Macromolecular Chemistry, University of Hamburg, Bundesstraße 45, D-20146 Hamburg, Germany
[b] Institute for Combustion Technology, RWTH Aachen University, Templergraben 64, D-52056 Aachen, Germany

ARTICLE INFO

Article history:
Received 23 May 2019
Revised 8 October 2019
Accepted 14 November 2019
Available online 30 November 2019

Keywords:
Droplet evaporation
Acoustic levitation
Acoustic streaming
Particle image velocimetry
Wet-bulb temperature

ABSTRACT

Acoustic levitation has been used successfully as a model system for spray polymerization processes and the determination of particle morphology. The experimental extension for the investigation of heat and mass transfer in levitated liquid droplets requires much more effort. In order to enable the levitation method as a universal tool for the tracking of heat and mass transfer, influencing experimental parameters and their effect on relevant characteristics like droplet deformation, temperature and surrounding flow field were analyzed. These parameters were elucidated experimentally to reveal their mutual dependencies. It was shown that the evaporation rate is affected by the aspect ratio of a droplet, which is directly correlated with its wet-bulb temperature. This was primarily explained by varying acoustic flow field patterns based on classical fluid mechanics, gas velocities and acoustic boundary layer thicknesses, which were visualized and quantified by particle image velocimetry. In order to study the wet-bulb temperature, thermocouple measurements on the levitated droplet were performed. It turned out, that the wet-bulb temperature is dependent on the power input and the resulting sound pressure level as it changes the acoustic field around the droplet. Moreover, the temperature measurement revealed the necessity to establish a temperature correction to account for heat conduction effects along the thermocouple shaft into the droplet. The illustrated experimental setup and measurement procedure is supposed to provide guidelines for the experimental determination of heat and mass transfer in evaporating droplets.

1. Introduction

The heat and mass transfer of liquid droplets in gaseous atmospheres has been studied widely for many decades and is of great interest in process engineering. There are many studies coping with the evaporation of single droplets under steady conditions or with externally forced gas convection for instance by an incident gas flow [1–4]. Monitoring droplet diameters and temperatures provides general insights into the evaporation process relevant for spray drying, spray cooling, crop spraying, painting, coating and even combustion purposes.

In order to study the heating and evaporation characteristics of liquid droplets, there are several approaches to get access for experimental investigations. These setups are sessile droplets [5], pendant droplets [6,7] or freely falling droplets [8]. The latter is limited to small droplets and volatile components with high evaporation rates due to the experimental effort [9], while the other methods incorporate surface interactions that influence the observed evaporation rate. An additional heat in- or output by filament, cannula or any other touching surface affects the droplet temperature and disturbs the evaporation rate.

On the contrary, levitation offers containerless and non-invasive experimental conditions for investigations on the heat and mass transfer of single droplets at elevated temperatures. There are many different levitation principles such as aerodynamic [10], acoustic [11], electrostatic [12], optical [13] and magnetic [14]. Acoustic levitation is the most commonly used and versatile method to measure the evaporation rate and temperature of almost any kind of liquid as pointed out by Priego-Capote and de Castro. [15] It was first described by Bücks and Müller [16] and was mainly implemented in research by the National Aeronautics and Space Administration (NASA) and European Space Agency (ESA) in the 1970s as it allows the positioning of droplets or particles under microgravity conditions. [11,17] The physical basis of this method is the generation of a standing acoustic wave counteracting

* Corresponding author.
E-mail address: Werner.Pauer@chemie.uni-hamburg.de (W. Pauer).

https://doi.org/10.1016/j.ijheatmasstransfer.2019.119057
0017-9310/

Nomenclature

A	surface area
a	*major axis*
A_R	*aspect ratio*
Ampl	*amplitude*
b	*minor axis*
d	diameter
F	*force*
h	*distance between sonotrode and reflector*
Le	Lewis number
Nu	Nusselt number
Pr	Prandtl number
$\dot{Q}$	heat flux
Re	Reynolds number
Sc	Schmidt number
Sh	Sherwood number
T	temperature
V	volume

Greek symbols

λ	wavelength

Subscripts

ax	*axial*
drop	droplet
gas	*gas*
rad	*radial*
TC	Thermocouple

gravitational forces in order to suspend objects in a gaseous atmosphere. Therefore, it is highly suitable for the investigation of single evaporating droplets serving as a model system for all kinds of spray processes. [18] The particle formation and the respective morphology has been successfully investigated for polymeric particles [19–23], nanoparticles [19,24] and sugar alcohols like mannitol even including porosity of the resulting particles. [25] In these cases, the resistance of heat and mass transport is based on the formation of a solid shell during the emergence of particles.

Compared to this, investigating the heat and mass transfer of levitated liquid droplets is much more complex due to liquid/gas interfaces, and acoustic forces and streaming affecting the droplet. The evaporation of droplets is well described in literature [26], especially for acoustically levitated droplets. [27] A recent review on droplet evaporation is given by Zhang et al. [28]. Empirical correlations for the Nusselt (*Nu*) and Sherwood (*Sh*) number were developed by Ranz and Marshall back in the 1950s for the evaporation of droplets including gas convection (Eqs. (1)+(2)) [29].

$$\mathrm{Nu} = 2 + 0.6\ \mathrm{Re}^{\frac{1}{2}}\ \mathrm{Pr}^{\frac{1}{3}} \tag{1}$$

$$\mathrm{Sh} = 2 + 0.6\ \mathrm{Re}^{\frac{1}{2}}\ \mathrm{Sc}^{\frac{1}{3}} \tag{2}$$

The Nusselt and Sherwood number can be described by the Reynolds (*Re*), Prandtl (*Pr*) and Schmidt (*Sc*) number. A value above two indicates an additional convection. An overview over other empirical correlations is given by Renksizbulut [30].

For acoustically levitated droplets, Yarin et al. calculated the acoustic radiation pressure based on the boundary element method to predict droplet shapes and a resulting droplet displacement in the acoustic field [31]. In further studies, the rates of heat and mass transfer of acoustically levitated droplets were modeled with regard to the acoustic streaming induced by the acoustic force field [27]. Schiffter and Lee described an increased mass transfer for evaporating droplets in comparison to boundary layer theory due to the acoustic streaming resulting in higher Sherwood numbers [32]. Zaitone et al. illustrated how the outer acoustic streaming affects the heat and mass transfer by analyzing the vapor distribution around a droplet using laser absorption spectrometry and comparing the droplet evaporation in an acoustic field versus a glass-filament [33,34]. Further publications coping with acoustic streaming and its influence on heat and mass transfer used particle image velocimetry (PIV) as visualization technique [4,35–38]. The typical inner and outer acoustic vortices were characterized as an induced convective gas motion around the droplets. The outer vortices can be eliminated by introducing an external gas blowing along the levitation axis. The droplets experienced a gas streaming with various Reynolds numbers to approach conditions that are close to those in spray systems [18].

Acoustically levitated droplets are deformed to oblate spheroids as the axial positioning force is approximately five times higher than the radial one [39]. The resulting aspect ratio of the droplet is an equilibrium between the surface pressure distribution and the surface tension of the levitated media. Loth describes the dependence of droplet deformation on the local Weber and Reynolds number [40]. The shape and instability of levitated droplets under high sound intensity and sound pressure level (SPL) conditions were studied experimentally and numerically by Lee et al. [41]. Di et al. created liquid films with aspect ratios up to 16 by increasing the SPL. Consequently, a pressure gradient is formed inside the film due to the buckled geometry and an enhanced suction effect of acoustic radiation pressure at the droplets rim, leading to the formation of a bubble [42]. The bubble formation can also be induced by tools like a needle or a rigid ring [43]. If the deformation of droplets by increased forces acting on the surface cannot be counteracted by surface tension, it can also result in the bursting of the droplet due to the capillary waves [17,44]. A recent study by Zaitone investigating the influence of the deformation of spheroids on their evaporation rate revealed that it still follows the d^2-law [45].

The evaporation of acoustically levitated droplets, the influence of acoustic streaming, and the deformation of droplets are well described in literature. Acoustic levitators are oftentimes custom-built and a precise comparison of evaporation data among different devices is only reasonable, if the specific acoustic field is taken into account. Generally, standing wave conditions are set empirically without any further differentiation. This study shows, that evaporation rates can differ up to 40% by manipulating the acoustic levitator settings. The consecutive effect of the droplet shape on acoustic streaming patterns and velocities resulting in a non-linear evaporation behavior has not been addressed in the literature, yet.

This work provides a sensible procedure for the determination of heat and mass transfer in acoustically levitated droplets. To point out considerable effects and sensitivities of an experimental acoustic levitation setup, a parametric study is performed. This study addresses adjustments in the acoustic field and their influences on the acoustic streaming pattern visualized by PIV technique affecting the respective droplet evaporation. The results are supposed to sensitize for experimentally based influences on evaporation data.

2. Experimental method

2.1. Setup of the acoustic levitator

Experiments concerning single droplet evaporation were carried out in a customized acoustic levitator with an insulated process chamber (Fig. 1). The key components were the ultrasonic processor (UIP25spec, 25 W, *Hielscher Ultraschall-Technologie*) using a piezoelectric transducer with a frequency of 42 kHz, a titanium horn as sonotrode (174 mm in length, 22 mm in diameter,

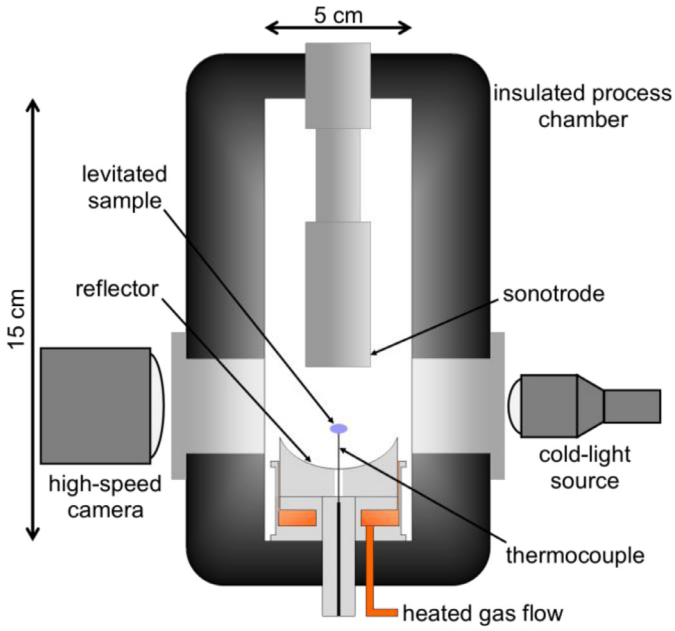

Fig. 1. Experimental setup, true to scale, of the custom-built acoustic levitator for the *on-line* analysis of levitated droplets. The droplet and gas temperature were measured at the same point within the pressure node.

≈90 mm deep inside the process chamber, *Ingo Jänich Ultraschall + Technologien*) and the concave reflector (33 mm inner diameter, radius of curvature 16.7 mm) that was positioned diametrically opposed. The distance between the horn and reflector could be adjusted by positioning tables (LTM 80–100-HSM, *OWIS GmbH*) with an accuracy of ±25 µm.

The setup was surrounded by an insulated process chamber (50 × 50 mm base, 150 mm in height) that allowed the adjustment of the gas temperature up to 250 °C by an implemented heating cable (*Horst GmbH*). The liquid sample of distinct volumes was injected into the pressure node using a microliter syringe (*Hamilton Bonaduz AG*) with a volume of 10 µL and an accuracy of ±0.1 µL.

The droplets were monitored *on-line* by shadowgraphy images taken by a CMOS high speed camera (1024 × 1024 pixels, 1 pixel = 3.78 µm, MotionPro Y4, *Integrated Design Tool Inc.*) providing images with a rate of up to 8 Hz. A micro-inspection lens system (Optem zoom 125, *Qioptiq*) was attached to the camera for magnification. The droplets were illuminated through a clouded polycarbonate window by a cold-light source (Technolight 270, *KARL STORZ GmbH & Co. KG*). An online data processing program written in LabVIEW (*National Instruments*) was used as a control software for measurement data acquisition with an analysis algorithm that utilized the shadowgraphy images to determine the major and minor axis length (±4% uncertainty) of the ellipsoidal shaped droplet. On that basis, the droplet surface and volume were calculated.

A thermocouple (IKT 015, IKT 025 and IKT 035, all type K, class 1, *ES Electronic Sensors GmbH*) with a diameter of 150/250/350 µm could be introduced through a hole in the reflector for temperature measurements of the levitated droplet. The thermocouples had a specified absolute error of less than ±1.5 °C. A potential temperature offset of the individual thermocouple was eliminated by calibration. Long-term measurements at constant surrounding temperature provided a standard deviation in temperature value below 0.1 °C.

Particle image velocimetry experiments were conducted with a double-pulsed Nd:YAG laser system (λ = 532 nm, pulse duration = 7 ns, BSL T 220, Quantel) and light section optics from ILA_5150 GmbH. Images were recorded by a CCD camera (1600 × 1200 pixels, PCO 1600, PCO AG) with an attached optic (Micro-Nikkor 105 mm, Nikon).

3. Results and discussion

The evaporation of acoustically levitated droplets depends on multiple influences like the acoustic force field, droplet deformation, and acoustic streaming. The interpretation of obtained evaporation data is complicated as these factors are mutually dependent and the complex relationships are not completely understood.

The following experiments were conducted with bi-distilled water as levitated media. Water with its relatively high surface tension was able to cover a broad range of experimental conditions and droplet shapes without being atomized. The shape of a droplet was influenced by adjusting the distance between sonotrode and reflector and varying the amplitude of the sonotrode.

3.1. Adjustment of droplet aspect ratio and its effect on wet-bulb temperature and evaporation behavior

Acoustically levitated droplets do not exhibit a perfectly spherical shape due to the applied inhomogeneous pressure field. The axial positioning forces F_{ax} exceed the radial positioning forces F_{rad} approximately by the factor 5 (Fig. 2). [39] As a result, the droplets are deformed to oblate spheroids with an increased surface area. The deformation, which can be determined by the acoustic Bond number Bo_a, mainly depends on the SPL acting onto the droplet surface and the surface tension of the liquid [42]. The resulting droplet shape is characterized by the aspect ratio a/b of the droplet, which is defined by the major axis a and the minor axis b (Fig. 2). The aspect ratio can be raised either by enhancing the SPL through increasing the amplitude of the sonotrode or by increasing the sound intensity through decreasing the distance between sonotrode and reflector [46]. The influence of gravity on the aspect ratio is negligible as pointed out by Xie and Wei [47].

The levitation of droplets is usually achieved by empirically applying conditions as close as possible to the standing acoustic wave condition. There are numerous combinations in levitator settings, which lead to a more or less stable levitation of droplets within the same pressure node, however, at varying aspect ratios.

The aspect ratio of a droplet is used as a directly quantifiable product of the applied acoustic pressure field. Adjusting the aspect

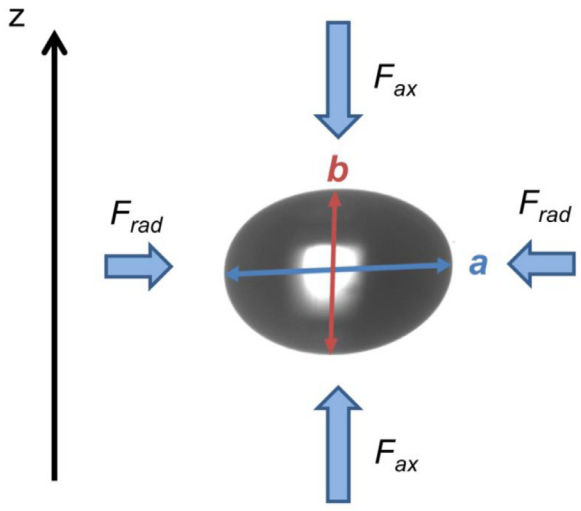

Fig. 2. Aspect ratio a/b (in this example 1.4) of an oblately deformed droplet defined by major axis a and minor axis b resulting from the inhomogeneous pressure field $F_{ax} > F_{rad}$.

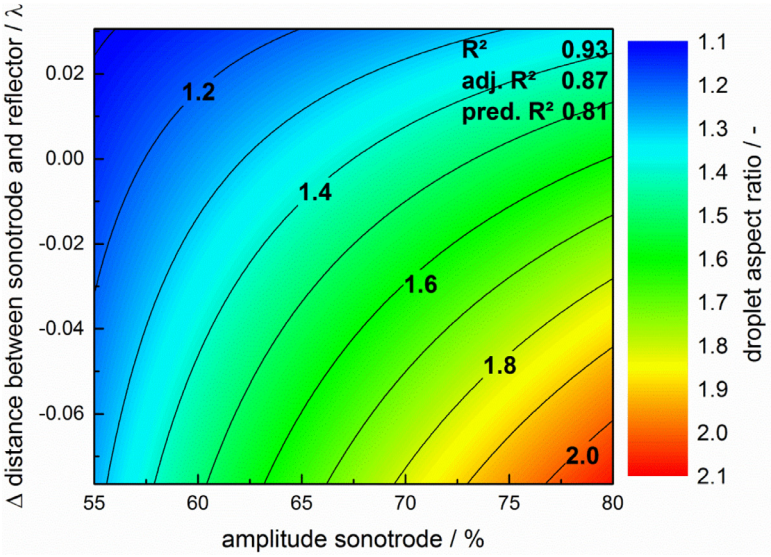

Fig. 3. Contour plot regarding the influence of the ultrasonic amplitude and sonotrode displacements in wavelength fractions λ on resulting water droplet ($V = 3.5$ µL) aspect ratio modeled by design of experiments (18 experiments).

ratio of a droplet can be achieved by manipulating the acoustic field either by changing the power (25 W in maximum) and therefore the amplitude of the sonotrode *Ampl* (39 µm at 100%, 16 µm at 50% peak to peak, respectively) or changing the distance between sonotrode and reflector *h*. A modulation in distance between sonotrode and reflector (Δh) is given in fractions of the wavelength ($\lambda = 8.17$ mm) with regard to the initial distance of 39.4 mm. This corresponds to a distance of 4.8 λ at the lowest point of the reflector. The curvature of the reflector provides a stable levitation at this distance despite the fact, that the distance does not formally fulfill the criteria of an being an integer number of half the wavelength. The influence of both factors on the aspect ratio of water droplets with an initial volume of 3.5 µL was evaluated with the help of design of experiments and statistical analysis at 70 °C gas temperature. The coded and normalized equation obtained by DoE enables a comparison of the individual influences (Eq. (3)). It reveals that the impact of the amplitude of the emitter exceeds the influence of the distance between sonotrode and reflector by 46% under the chosen experimental conditions. Additionally, the aspect ratio is affected by an interaction term.

$$a/b = 1.43 + 0.2639 \cdot Ampl - 0.1809 \cdot h - 0.1332\, Ampl \cdot h \qquad (3)$$

It is possible to alter the droplet aspect ratio inside the same pressure node precisely by manipulating the levitator settings (Fig. 3). A slight deviation from acoustic wave resonance conditions can be overcome by adjusting the power and thereby the sonotrode amplitude. This coupling clarifies the diversity of evaporation conditions if not further defined. The value for R^2 of 0.93 being close to the adjusted R^2 of 0.87 proves a good and significant model regarding the studied influences on the droplet aspect ratio. The aspect ratio of water droplets increases almost linearly up to 2.1 by decreasing the distance between sonotrode and reflector by 0.077 λ compared to regularly applied standing wave conditions and raising the amplitude to 80%. Almost spherical droplets with an axial ratio of 1.1 can be generated by low amplitude values and increasing the distance between sonotrode and reflector. However, the lowest limit of acoustic forces for the compensation of gravitational forces is reached in this area and the experimental feasibility is not guaranteed for all combinations.

A higher energy input entails a higher aspect ratio, which increases the surface-area-to-volume ratio of the droplet. This influences the heat and mass transfer as they occur at the interface between the liquid and the gaseous phase. This effect can be determined by investigating the wet-bulb temperature of droplets with varying aspect ratios. The wet-bulb temperature of the droplet is exhibited due to the equilibrium between heat transfer and evaporative cooling, which leads to a constant droplet temperature over time. The droplet temperature, however, is the measured temperature, that includes influences by the measurement technique. The droplet temperature was measured by a thermocouple (150 µm in diameter) and corrected based on Fig. 11 in order to obtain the wet-bulb temperature. A temperature measurement by IR-thermography as implemented by Tuckermann [48] cannot be applied at elevated temperatures inside the process chamber due to surface reflections of heat radiation. The influence of the local power input due to sonotrode amplitude and the distance between sonotrode and reflector on the wet-bulb temperature of water droplets was investigated with an initial volume of 3.5 µL (Fig. 4). The evaluation was based on design of experiments and statistical analysis at 70 °C gas temperature. The normalized and transformed equation shows that the influence of the amplitude exceeds the effect of the distance between sonotrode and reflector by 17%. The same parameters and their combination being statistically significant in Eqs. (3) and (4) show a direct linkage between the aspect ratio and the droplet temperature. Consequently, the droplet temperature can be determined based on the aspect ratio of the respective droplet independently from the specific levitator parameters.

$$T^3 = 17601.94 + 1162.49 \cdot Ampl - 989.54 \cdot h - 1152.26 \cdot Ampl \cdot h \qquad (4)$$

The wet-bulb temperatures varies from 21.5 °C at lower acoustic forces to 23.5 °C at higher forces due to higher sonotrode amplitudes and shorter distances between sonotrode and reflector. The measured temperature values are corrected by −4.8 K according to the finding in Fig. 12 in order to obtain the wet-bulb temperature.The obtained significant model with an R^2 of 0.91 and an adjusted R^2 of 0.88 reveals a dependence of the wet-bulb temperature on both parameters alternating the acoustic force field.

The wet-bulb temperature of a droplet is influenced by the acoustic radiation pressure (Fig. 5). The pressure distribution field is simulated with COMSOL® based on the initial distance between sonotrode and reflector of 39.4 mm. An additional surface averaged radiation pressure amounts 3.25 kPa at an amplitude of 55% and 5.3 kPa at an amplitude of 80%. The difference of 2.05 kPa yields an

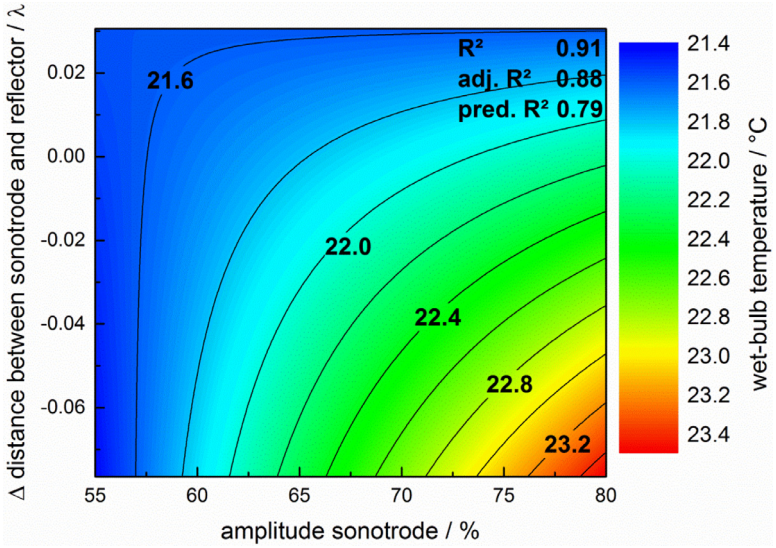

Fig. 4. Contour plot of the influence of ultrasonic amplitude and sonotrode displacements in fractions of the wavelength λ on resulting water droplet ($V = 3.5$ µL) wet-bulb temperature modeled by design of experiments (18 experiments). The temperature is corrected by −4.8 °C according to Fig. 11.

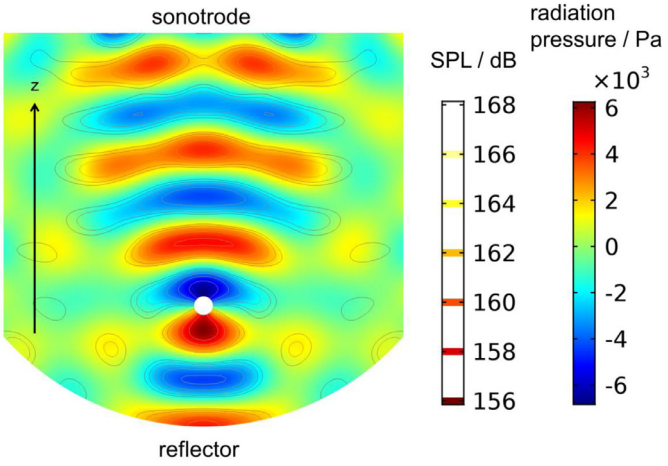

Fig. 5. Acoustic radiation pressure distribution and resulting SPL inside the levitator with inserted spherical water droplet (V_{drop} = 3.5 µL, *Ampl* = 70%, T_{gas} = 70 °C).

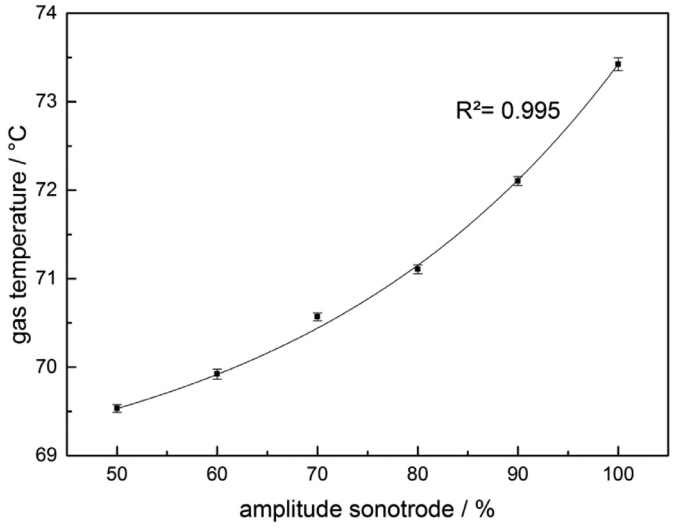

Fig. 6. Influence of the amplitude of the sonotrode on resulting gas temperature within the pressure node with standard deviation. Temperature measurements were done by thermocouple according to Fig. 1.

increase in wet-bulb temperature of 0.2 °C within the experimental settings [49,50]. This explains 10% of the increase in wet-bulb temperature as seen in Fig. 4.

An increased gas temperature in the droplet surrounding (Fig. 6) was found as another valid explanation for the varying wet-bulb temperature. A higher amplitude of the sonotrode increases the sound pressure level, which leads to an increase of evaporation rate according to the results of Bänsch and Götz. [51] Additionally, the process chamber of the levitator contains a temperature gradient as it is heated by heating wires through the chamber walls. The gas temperature decreases gradually towards the non-heated center, where additional gas convection was induced by the acoustic force field (Fig. 8). This gas convection leads to significant changes in gas temperatures within the pressure node (Fig. 6). An increase in gas temperature of 1.5 K within the experimental window used in Figs. 3 and 4 results in a 3% higher evaporation rate based on a statistical evaluation of evaporation data by Hellwig. [52] A further quantification of this effect on droplet temperature is renounced as the gas temperature measurements were done without a droplet in the acoustic field. Acoustic wave reflections on the surface of a droplet have further impact on gas patterns and temperature values. Trinh and Robey published the influence of acoustic gas convection on a heated thermistor for further information [36].

Both statistical models for the wet-bulb temperature (Fig. 4) and the aspect ratio (Fig. 3) exhibit the same trend and show a direct correlation of these two target parameters. A higher droplet deformation entails an increase in wet-bulb temperature. This behavior is not intuitive as an increase in surface-area-to-volume ratio could lead to an equally improved heat and mass transfer resulting in the same temperature.

Higher aspect ratios cause an increase in evaporation rate of the respective droplet (Fig. 7). The evaporation rate was calculated based on the temporal evolution of the squared sphere equivalent diameter which corresponds with the slope according to the d^2-law by Law and Law [3]. It was further normalized with respect to the evaporation rate of a droplet as close as possible to a perfectly spherical shape ($a/b = 1.09$). Although the ambient conditions were not changed, an increased normalized evaporation rate of up to 40% can be observed at an aspect ratio of 1.6

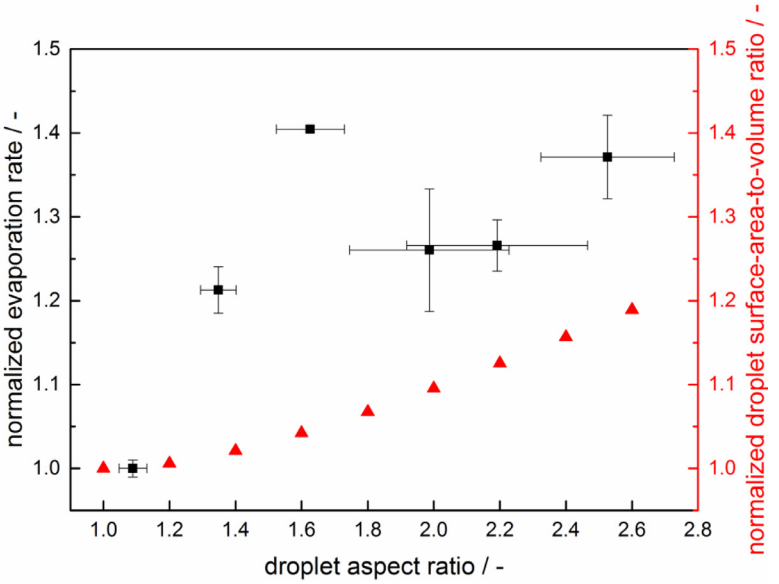

Fig. 7. Influence of the droplet aspect ratio on resulting normalized evaporation rate and normalized surface-area-to-volume ratio of acoustically levitated water droplets ($V = 2$ µL, gas temperature 60 °C). Measurement points are based on four individual droplets at minimum with their respective standard deviation. The standard deviation of the droplet aspect ratio increases with higher values as the acoustic force was kept constant in contrast to investigations of Zaitone [45].

compared to almost spherical droplets. A possible explanation of the rise in normalized evaporation rate can be provided by a higher surface-area-to-volume ratio and the associated increase in heat and mass transport. This is analogous to an increase in normalized evaporation rate for decreasing droplet sizes as shown by Verwey and Birouk [53]. The surface-area-to-volume ratio is calculated based on a rotationally symmetric elliptic droplet geometry. The increase in evaporation rate at higher aspect ratios exceeds the rise in surface-area-to-volume ratio. A reason for this behavior is provided by a higher acoustic radiation pressure (Fig. 5), a higher surrounding gas temperature (Fig. 6) and a larger wet-bulb temperature of the droplet (Fig. 4) at bigger aspect ratios. However, the non-linear behavior at low aspect ratios with a local maximum at an aspect ratio of 1.6 cannot be explained by the identified effects, yet. An explanation is provided by changes in acoustic flow field characteristics and streaming velocities, that are accompanied by varying convective heat and mass transfer.

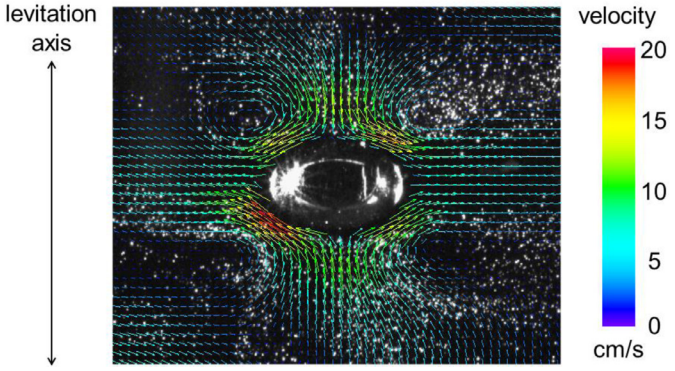

Fig. 8. Acoustically levitated water droplet ($V = 2$ µL) with tracer particle seeding in the gaseous phase and superimposed streaming velocity vectors obtained by PIV analysis.

3.2. Acoustic flow field characteristic in the surrounding of oblate droplets

Different acoustic pressure fields and resulting droplet shapes lead to various acoustic streaming characteristics. On the one hand, the acoustic wave reflection pattern changes with droplet shape. On the other hand, the induced gas flow due to acoustic streaming impinges on different droplet curvatures resulting in different deflection patterns.

The analysis of the flow field around levitated water droplets by PIV (Fig. 8) proves the existence of the characteristic acoustic vortices described by Yarin [27]. The inner acoustic streaming is located at the surface boundary, while the outer acoustic streaming is represented by the toroidal vortices.

The incident gas flow approaches the droplet diametrical opposed in direction of the levitation axis over the entire width of the droplet. The gas flow with the mean velocity of 10 cm/s is accelerated to a maximum of 19 cm/s after being deflected by the droplet ($V = 2$ µL, aspect ratio = 1.8, d_m = 2.1 mm) into two streaming channels, each with a diameter of approximately 500 µm. Having surpassed the droplet surface, the gas leaves into the bulk orthogonally to the levitation axis with a reduced velocity.

The comparison of the flow velocity vectors in the surrounding of droplets at different aspect ratios reveals that the gas velocity increases with higher aspect ratio (Fig. 9). The incident flow velocities approaching the droplets from the top is averaged along the entire droplet width. In a distance of 555 ± 25 µm in front of the droplet surface, the mean gas velocity ranges from 7.0 cm/s at an aspect ratio of 1.2–12.5 cm/s at an aspect ratio of 3.1 (Table 1). The velocity distribution of the gas along the droplet width, each referred to a droplet of an aspect ratio of 1.2 ($a = 1.87$ mm), is given in Fig. 9. A normally distributed velocity field was obtained exhibiting a laminar flow behavior in the droplet surrounding.

At high aspect ratios of 3.1 (Fig. 9c), a steady boundary layer with a thickness of 200 µm was formed around the droplet that was not present at an aspect ratio of 1.8 (Fig. 9b). This can be explained by the generation of a stagnation point as the gas flow impinges onto the droplet surface in an angle close to 90°. An almost spherical droplet (aspect ratio 1.2, Fig. 9a) formed a stall of the flow, where the gas does not follow the whole curvature of the droplet. This results in an area with a low gas velocity in

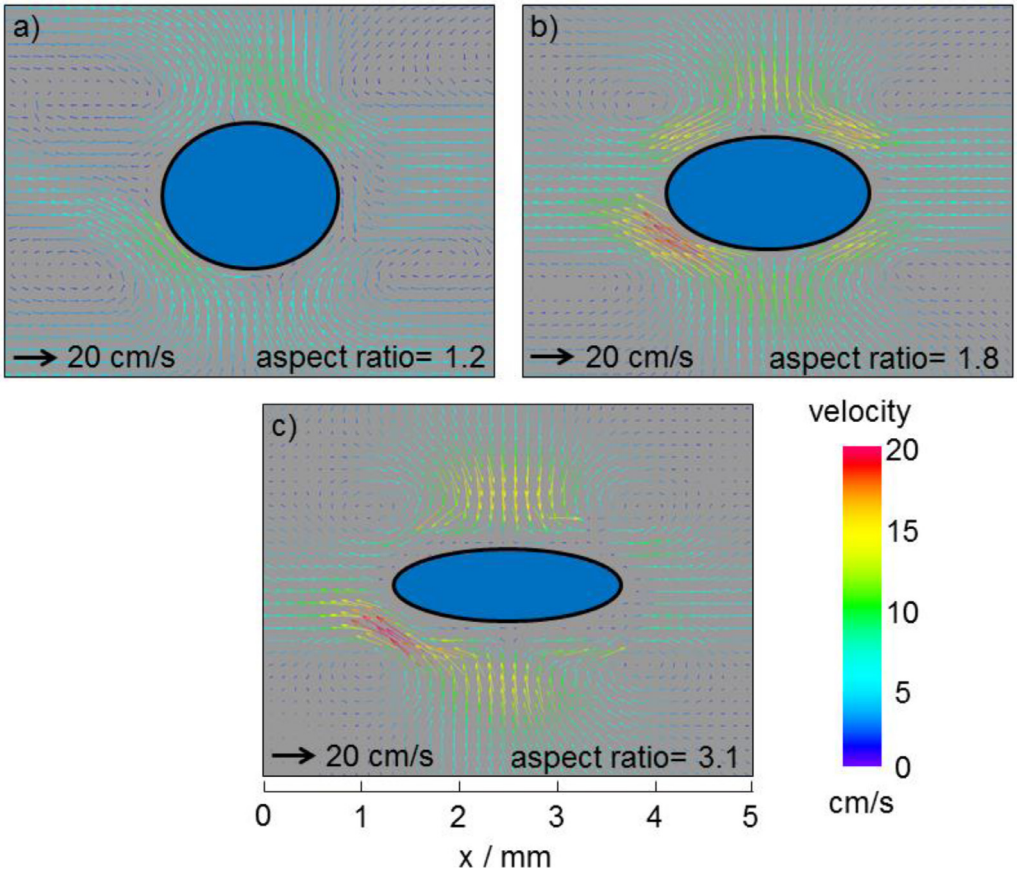

Fig. 9. Acoustic flow field around a levitated water droplet ($V = 2$ µL) with an aspect ratio of 1.2 (a), 1.8 (b) and 3.1 (c). Velocity vectors were derived by calculating the mean velocity of at least 19 image pairs taken with 2 Hz.

Table 1
Mean incident flow velocity and resulting Reynolds, Nusselt and Sherwood number for water droplets at different aspect ratios.

Aspect ratio	Major axis / mm	Mean incident flow velocity / cm/s	*Re* number	Nu/Sh number
1.2	1.87	7.0	9.1	3.6
1.8	2.05	10.2	14.5	4.0
3.1	2.37	12.5	20.6	4.4

equatorial direction. In this case, the outer areas of the toroidal vortices, visible by an enriched tracer particle density, were located in a distance of 500 µm to the droplet surface, while the distance was halved to 250 µm at higher aspect ratios.

The inner acoustic streaming at the surface boundary layer provides a forced convection that results in a higher heat and mass transfer, while the outer acoustic vortices accumulate evaporated liquid, that inhibits further evaporation processes. Referring to the findings of Fig. 7, a disproportionate increase in evaporation rate up to 40% at an aspect ratio of 1.6 compared to an almost spherical droplet can be explained by an enhanced gas velocity at the surface boundary layer (compare Fig. 10) resulting in higher *Re* numbers (Table 1). Another contribution to a higher evaporation rate is a streaming pattern following the droplet curvature more closely instead of forming a stall and an area of low gas velocity at the edge of the droplet in horizontal direction. A decrease in evaporation rate at higher aspect ratios around 2.0 (compare Fig. 7) could be explained by the absence of a boundary layer due to a stagnation point with very low gas velocities as observed at a droplet with an aspect ratio of 3.1 (Fig. 9c). As the gas velocity increases at higher aspect ratios due to the higher energy input, a further rising evaporation rate can be explained by the higher Reynolds numbers and a larger surface-area-to-volume ratio, as well. These first experimentally based interpretations are supposed to be validated with further PIV measurements in a finer resolution of aspect ratios in the future.

The Reynolds numbers ranging from 9.1 to 20.6 for aspect ratios of 1.2 and 3.1, respectively, were calculated based on the mean incident flow velocity 550 ± 25 µm in front of the droplet surface and the droplet major axis a as characteristic length. This was done as an estimation of an averaged velocity that is lower at the poles and the equator of the oblate droplet and higher in areas of higher curvature in between. The characteristic Nusselt and Sherwood numbers at different aspect ratios were calculated based on the correlations of Ranz and Marshall (Equations (1)+(2)) [29]. As the Schmidt and Prandtl number are constant and resulted in a Lewis (Le) number of ≈1, Nusselt and Sherwood number are solely depending on the Reynolds number. Nusselt and Sherwood number increase from 3.6 at an aspect ratio of 1.2–4.4 at a higher aspect ratio of 3.1 (Table 1). This fact, in combination with the alternating streaming patterns, the wet-bulb temperature being dependent on the aspect ratio (compare Fig. 4), the gas temperature being

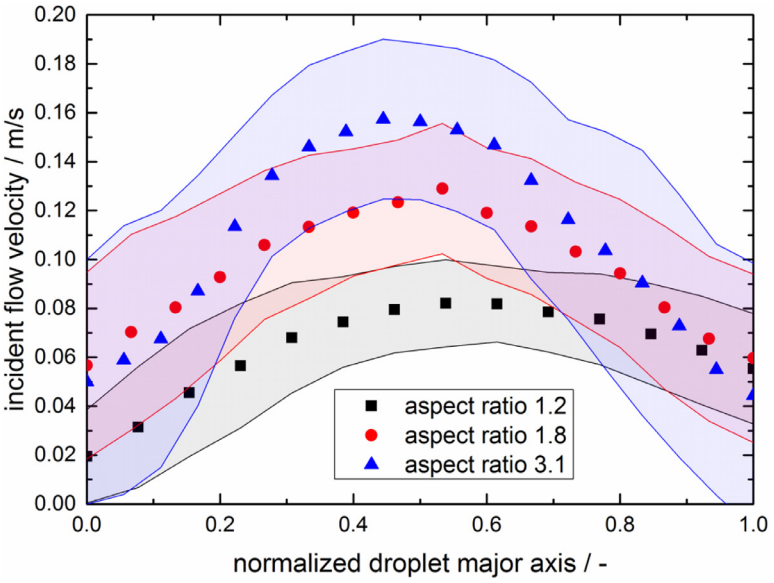

Fig. 10. Flow velocity distribution approaching an acoustically levitated water droplet ($V = 2$ µL) from the top along the droplet width, each referred to an aspect ratio of 1.2 ($a = 1.87$ mm), in a distance of 550 ± 25 µm with standard deviation.

dependent on the energy input and the general change in surface-area-to-volume ratio of oblate droplets explains the characteristic behavior in evaporation rate observed in Fig. 7 for different aspect ratios.

Models concerning the evaporation of oblately deformed droplets are supposed to be extended to reproduce the non-linear relation of the evaporation rate at different aspect ratios. This can be done by more extensive experimental validations over a broader range of aspect ratios in order to refine models, for example from Zaitone [45,54]. Afterwards, the model takes into account that the acoustic streaming velocity and the flowing pattern change as the aspect ratio is adjusted by modulating the acoustic field. In a free gaseous medium without acoustic streaming, the evaporation rate would monotonically increase at rising aspect ratios due to the higher surface-area-to-volume ratio.

3.3. Temperature measurement of evaporating droplets

An adequate measurement of the droplet temperature is essential for the determination of heat and mass transfer in a levitated droplet. The temperature data was obtained by inserting a thermocouple with a diameter of 150 µm inside the droplet near its center. The thermocouple measurement causes an accelerated evaporation by 6 ± 4% compared to freely levitated droplets at a gas temperature of 70 °C. A more precise quantification is not possible as the thermocouple generally tends to lower the aspect ratio of a deformed droplet leading to changes in ambient conditions as already discussed. Due to this fact, the increasing evaporation rate might be underestimated as the evaporation rate decreased at lower aspect ratios below 1.6 according to Fig. 7 by superimposing the additional heat conduction provided by the thermocouple. Additional PIV measurements in the droplet surrounding with inserted thermocouple and inside a deformed droplet could provide insights into alterations concerning heat and mass transfer. However, at this point, the increase in evaporation rate overlaps with the image based significance threshold of 4%, thus only indicating an influence of the thermocouple due to additional heat conduction, especially at higher temperatures. Consequently, the invasive temperature measurement method is expected to induce an additional heat transfer, which has to be considered (Fig. 11).

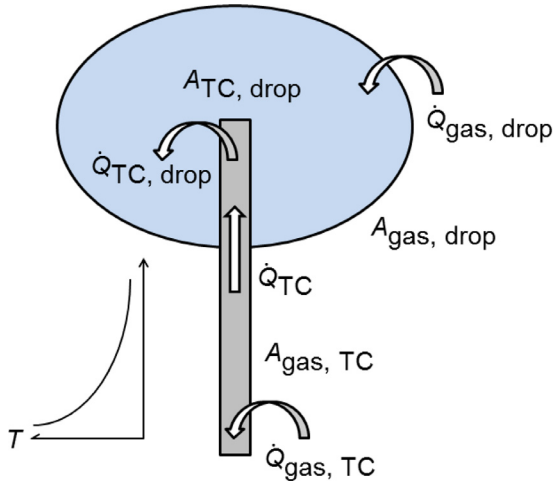

Fig. 11. Heat transfer due to invasive droplet temperature measurement by thermocouple including important heat fluxes, interface areas and the temperature gradient within the thermocouple.

The thermocouple enhances the heat transfer area as the heat exchange does not only take place at the interface between droplet and gas $A_{gas,\,drop}$, but also at the interface between thermocouple and gas $A_{gas,\,TC}$. A conductive heat flux into the droplet Q_{TC} along the stainless steel covered thermocouple is formed, that enhances the droplet temperature. This effect is expected to increase with higher difference between droplet and gas temperature.

The experimental estimation of the heat flux along the thermocouple axis was performed by measuring the droplet temperature of water droplets with structurally identical thermocouples (Type K, Class A, Electronic Sensor) with different diameters ranging from 150 to 350 µm. The detected water droplet temperature increases linearly with the diameter of the inserted thermocouples from 24.0 °C for a diameter of 150 µm by 6.3 °C to a maximum of 30.3 °C for the 350 µm thermocouple (Fig. 12). By extrapolating the data, an intercept point at 19.2 °C at the droplet temperature axis is obtained as the wet-bulb temperature for these conditions. As a result, the obtained data by the invasive 150 µm thermocouple is supposed to be corrected by adjusting the value for aqueous

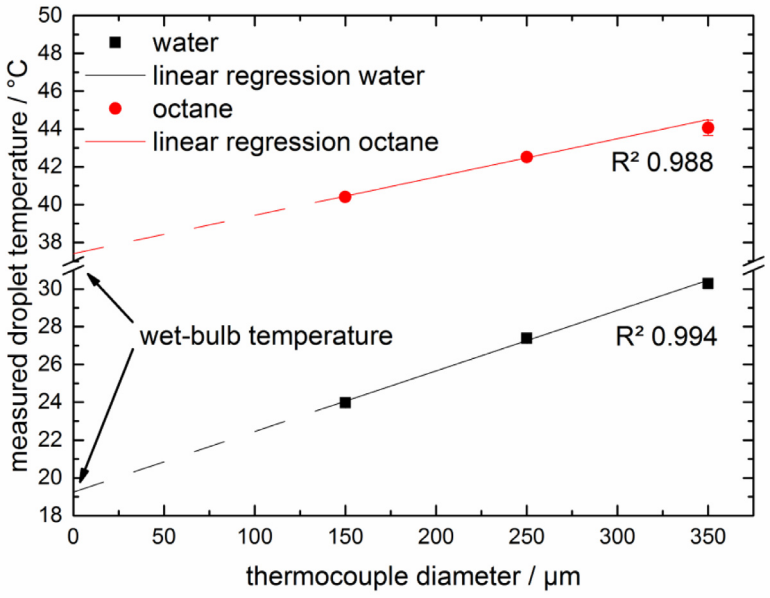

Fig. 12. Influence of thermocouple size on the measured temperature of water and octane droplets at a gas temperature of 62 °C with standard deviation and extrapolated wet-bulb temperature.

droplets by −4.8 K to receive the wet-bulb temperature. A correction of −4.0 K is obtained by applying the same method for organic octane droplets. These findings are in great accordance with the data of Downing, [6] who correlated the wet-bulb temperature for evaporating pendant droplets in a heated air stream. The linearity of the measured data shows, that the heat transfer is limited by the surface of the thermocouple and therefore the interface area with the gaseous atmosphere. A quadratic dependence would speak for a limitation by the cross-sectional area of the thermocouple and thus the heat conduction along the axis into the droplet.

It is known that levitated droplets exhibit complex flow patterns, which provide mixing within the droplet [35,55,56]. The inserted thermocouple could cause turbulences, which increase the droplet mixing or act like a flow breaker to suppress fluid circulation. This impact is supposed to be strongly dependent on the size of the thermocouple and the droplet. These effects of the invasive measurement technique have not been further investigated yet.

3.4. Recommendations for valid evaporation measurements of levitated droplets

In order to obtain reliable results concerning the heat and mass transfer of acoustically levitated droplets, several experimentally based details should be ensured. First of all, the acoustic pressure field is fixed by a constant distance between sonotrode and reflector and a constant sonotrode amplitude. Based on this, the levitated droplets inside the chosen pressure node exhibit a certain aspect ratio, ideally close to spherical droplets of around 1.2. This aspect ratio reduces the influence of convective heat and mass transfer due to the acoustic streaming, while still counteracting gravitational forces to ensure a stable levitation process. It is important to compare data of droplets with the same aspect ratio, because changes in evaporation rate might stem from different acoustic streaming patterns and gas velocities and not from the objective parameter. Otherwise, detailed knowledge about the acoustic streaming patterns is mandatory. The gas temperature inside the pressure node is dependent on the sound pressure level and streaming pattern due to a temperature gradient, if the process chamber is solely heated through the walls. An external pre-heated gas flow can diminish the temperature gradient inside the process chamber.

Temperature measurements should be done by a thermocouple as small as possible in diameter to reduce heat conduction into the droplet. Alternatively, Raman thermometry [57,58] or planar laser-induced fluorescence [59] could provide contactless temperature measurement methods at a more extensive effort, though.

4. Conclusions

This study pointed out the interdependencies of the experimental setup parameters of an acoustic levitator, the resulting droplet shape and its impact on acoustic streaming and the respective heat and mass transfer.

The aspect ratio of a droplet was the result of the characteristic acoustic force field set by the sonotrode amplitude and the distance between sonotrode and reflector. Models obtained by design of experiments revealed that the droplet temperature was linked to the aspect ratio of the respective droplet and increased up to 2 °C at higher aspect ratios. However, the evaporation rate was not proportional to droplet deformation and the respective surface-area-to-volume changes and experienced discrepancies of 40% in maximum. This was explained by a higher surrounding gas temperature and changing flow field patterns of the inner acoustic streaming as visualized by PIV measurements. Additionally, a detaching of the gas stream along the droplet curvature at low aspect ratios and the formation of a boundary layer due to a stagnation point around the whole droplet at high aspect ratios occurred. Acoustic streaming velocities were proved to increase at higher aspect ratios resulting in higher Reynolds and consequently higher Sherwood and Nusselt numbers. Heat conduction along the axis of the thermocouple was accounted for by correcting the measured temperature by data extrapolation in great accordance with literature data [6] in order to gain the wet-bulb temperature of the evaporating droplet. Finally, general recommendations for valid evaporation measurements of acoustically levitated droplets were provided.

Funding sources

This research did not receive any specific grant from funding agencies in the public, commercial, or not-for-profit sectors.

Declaration of Competing Interest

None

Acknowledgement

The authors like to thank DANTEC DYNAMICS for their support concerning the evaluation of the PIV images.

References

[1] G. Brenn, L.J. Deviprasath, F. Durst, C. Fink, Evaporation of acoustically levitated multi-component liquid droplets, Int. J. Heat Mass Transf. 50 (2007) 5073–5086, doi:10.1016/j.ijheatmasstransfer.2007.07.036.
[2] M. Mezhericher, A. Levy, I. Borde, Theoretical models of single droplet drying kinetics: a review, Drying Technol. 28 (2010) 278–293, doi:10.1080/07373930903530337.
[3] C.K. Law, H.K. Law, A d^2-Law for multicomponent droplet vaporization and combustion, AIAA J. 20 (1981) 522–527, doi:10.2514/3.51103.
[4] K. Shitanishi, K. Hasegawa, A. Kaneko, Y. Abe, Study on heat transfer and flow characteristic under phase-change process of an acoustically levitated droplet, Microgravity Sci. Technol. 26 (2014) 305–312, doi:10.1007/s12217-014-9401-1.
[5] H.Y. Erbil, Evaporation of pure liquid sessile and spherical suspended drops: a review, Adv. Colloid Interface Sci. 170 (2012) 67–86, doi:10.1016/j.cis.2011.12.006.
[6] C.G. Downing, The evaporation of drops of pure liquids at elevated temperatures: rates of evaporation and wet-bulb temperatures, AIChE J. 12 (1966) 760–766, doi:10.1002/aic.690120424.
[7] K. Chuchottaworn, P. Fujinami, A. Asano, Experimental study of evaporation of a volatile pendant drop under high mass flux conditions, J. Chem. Eng. Jpn. (1984) 599, doi:10.1252/jcej.17.7.
[8] H.A. Duguid, J.F. Stampfer, The evaporation rates of small, freely falling water drops, J. Atmos. Sci. 28 (1971) 1233–1243, doi:10.1175/1520-0469(1971)028⟨1233:TEROSF⟩2.0.CO;2.
[9] J. Wilms, Evaporation of multicomponent droplets, Universität Stuttgart (2005).
[10] P.C. Nordine, R.M. Atkins, Aerodynamic levitation of laser-heated solids in gas jets, Rev. Scient. Instrum. 53 (1982) 1456–1464, doi:10.1063/1.1137196.
[11] E.H. Trinh, Compact acoustic levitation device for studies in fluid dynamics and material science in the laboratory and microgravity, Rev. Scient. Instrum. 56 (1985) 2059–2065, doi:10.1063/1.1138419.
[12] P.F. Paradis, T. Ishikawa, S. Yoda, Electrostatic levitation research and development at JAXA: past and present activities in thermophysics, Int. J. Thermophys. 26 (2005) 1031–1049, doi:10.1007/s10765-005-6683-y.
[13] R.C. Gauthier, S. Wallace, Optical levitation of spheres: analytical development and numerical computations of the force equations, J. Opt. Soc. Am. B 12 (1995) 1680, doi:10.1364/JOSAB.12.001680.
[14] M.V. Berry, A.K. Geim, Of flying frogs and levitrons, Eur. J. Phys. 18 (1999) 307–313, doi:10.1088/0143-0807/18/4/012.
[15] F. Priego-Capote, L. de Castro, Ultrasound-assisted levitation: lab-on-a-drop, TrAC Trends Anal. Chem. 25 (2006) 856–867, doi:10.1016/j.trac.2006.05.014.
[16] K. Bücks, H. Müller, Über einige beobachtungen an schwingenden piezoquarzen und ihrem schallfeld, Zeitschrift Für Physik 84 (1933) 75–86, doi:10.1007/BF01330275.
[17] E.G. Lierke, Deformation and displacement of liquid drops in an optimized acoustic standing wave levitator, Acta Acustica United Acustica 88 (2002) 206–217 http://www.ingentaconnect.com/content/dav/aaua/2002/00000088/00000002/art00008.
[18] A.L. Yarin, G. Brenn, J. Keller, M. Pfaffenlehner, E. Ryssel, C. Tropea, Flow-field characteristics of an aerodynamic acoustic levitator, Phys. Fluids 9 (1997) 3300–3314, doi:10.1063/1.869444.
[19] R. Sedelmayer, M. Griesing, A.H. Halfar, W. Pauer, H.U. Moritz, Experimental investigation of the morphology formation of polymer particles in an acoustic levitator, Macromol. Symp. 333 (2013) 142–150, doi:10.1002/masy.201300088.
[20] J. Laackmann, W. Säckel, L. Cepelyte, K. Walag, R. Sedelmayer, F. Keller, W. Pauer, H.U. Moritz, U. Nieken, Experimental investigation and numerical simulation of spray processes, Macromol. Symp. 302 (2011) 235–244, doi:10.1002/masy.201000091.
[21] A.H. Halfar, W. Pauer, H.-.U. Moritz, Polymerization of partially neutralized acrylic acid in acoustically levitated droplets, ILASS - Europe 2014, 26th Annual Conference on Liquid Atomization and Spray Systems, 2014.
[22] D. Wong, T. Hellwig, A.H. Halfar, H.-.U. Moritz, W. Pauer, Design of particle morphology for redox-initiated spray polymerization of acrylic acid and sodium acrylate by investigating levitated single droplet, Macromol. Symp. 370 (2016) 128–134, doi:10.1002/masy.201600149.
[23] K. Franke, H.-.U. Moritz, W. Pauer, Beeinflussung der eigenschaften von sprühpolymerisationsprodukten, Chemie Ingenieur Technik 89 (2017) 490–495, doi:10.1002/cite.201600141.
[24] S. Basu, E. Tijerino, R. Kumar, Insight into morphology changes of nanoparticle laden droplets in acoustic field, Appl. Phys. Lett. (2013) 102, doi:10.1063/1.4801502.
[25] H. Grosshans, M. Griesing, M. Mönckedieck, B. Walther, S.R. Gopireddy, R. Sedelmayer, W. Pauer, H.-.U. Moritz, N.A. Urbanetz, E. Gutheil, Numerical and experimental study of the drying of bi-component droplets under various drying conditions, Int. J. Heat Mass Transf. 96 (2016) 97–109, doi:10.1016/j.ijheatmasstransfer.2015.12.062.
[26] E. Tsotsas, A.S. Mujumdar, Modern Drying Technology Volume 2: Experimental Techniques, Wiley-VCH, Weinheim, 2009.
[27] A.L. Yarin, G. Brenn, O. Kastner, D. Rensink, C. Tropea, Evaporation of acoustically levitated droplets, J. Fluid Mech 399 (1999) 151–204, doi:10.1017/S0022112099006266.
[28] D. Zang, S. Tarafdar, Y.Y. Tarasevich, M. Dutta Choudhury, T. Dutta, Evaporation of a droplet: from physics to applications, Phys. Rep. 804 (2019) 1–56, doi:10.1016/j.physrep.2019.01.008.
[29] W.E. Ranz, J.R. Marshall, Evaporation from drops, Chem. Eng. Progress 48 (1952) 173–180.
[30] X.L.M. Renksizbulut, R. Nafziger, A mass transfer correlation for evaporation in high-temperature droplet flows, Chem. Eng. Sci. (1991) 46, doi:10.1016/0009-2509(91)85133-I.
[31] A.L. Yarin, M. Pfaffenlehner, C. Tropea, On the acoustic levitation of droplets, J. Fluid Mech. 356 (1998) 65–91, doi:10.1017/S0022112097007829.
[32] H. Schiffter, G. Lee, Single-Droplet evaporation kinetics and particle formation in an acoustic levitator . Part 1: evaporation of water microdroplets assessed using boundary-layer and acoustic levitation theories, J. Pharm. Sci. 96 (2007) 2274–2283, doi:10.1002/jps.
[33] B.A. Zaitone, S. Hunsmann, G. Castanet, N... Damaschke, V. Ebert, C. Tropea, Evaporation of an acoustically levitated droplet, ICLASS, 2006.
[34] B. Ali Al Zaitone, C. Tropea, Evaporation of pure liquid droplets: comparison of droplet evaporation in an acoustic field versus glass-filament, Chem. Eng. Sci. 66 (2011) 3914–3921, doi:10.1016/j.ces.2011.05.011.
[35] K. Hasegawa, Y. Abe, A. Fujiwara, Y. Yamamoto, K. Aoki, External flow of an acoustically levitated droplet, Microgravity Sci. Technol 20 (2008) 261–264, doi:10.1007/s12217-008-9025-4.
[36] E.H. Trinh, J.L. Robey, Experimental study of streaming flows associated with ultrasonic levitators, Phys. Fluids 6 (1994) 3567–3579, doi:10.1063/1.868415.
[37] K. Hasegawa, Y. Abe, A. Kaneko, Y. Yamamoto, K. Aoki, Visualization measurement of streaming flows associated with a single-acoustic levitator, Microgravity Sci. Technol. (2009) 21, doi:10.1007/s12217-009-9134-8.
[38] K. Kobayashi, A. Goda, K. Hasegawa, Y. Abe, K. Kobayashi, A. Goda, K. Hasegawa, Y. Abe, Flow structure and evaporation behavior of an acoustically levitated droplet, Phys. Fluids (2018) 30, doi:10.1063/1.5037728.
[39] R. Tuckermann, B. Neidhardt, S. Bauerecker, Levitation in ultraschallfeldern, Physik Unserer Zeit 2 (2001) 69–75, doi:10.1002/1521-3943(200103)32:2⟨69::AID-PIUZ69⟩3.0.CO;2-#.
[40] E. Loth, Quasi-steady shape and drag of deformable bubbles and drops, Int. J. Multiph. Flow 34 (2008) 523–546, doi:10.1016/j.ijmultiphaseflow.2007.08.010.
[41] C.P. Lee, A.V. Anilkumar, T.G. Wang, Static shape and instability of an acoustically levitated liquid drop, Phys. Fluids A 3 (1991) 2497–2515, doi:10.1063/1.858192.
[42] W. Di, Z. Zhang, L. Li, K. Lin, J. Li, X. Li, B.P. Binks, X. Chen, D. Zang, Shape evolution and bubble formation of acoustically levitated drops, Phys. Rev. Fluids 3 (2018) 103606, doi:10.1103/PhysRevFluids.3.103606.
[43] D. Zang, L. Li, W. Di, Z. Zhang, C. Ding, Z. Chen, W. Shen, B.P. Binks, X. Geng, Inducing drop to bubble transformation via resonance in ultrasound, Nat. Commun. 9 (2018) 3546, doi:10.1038/s41467-018-05949-0.
[44] A.V. Anilkumar, C.P. Lee, T.G. Wang, Stability of an acoustically levitated and flattened drop: an experimental study, Phys. Fluids A 5 (1993) 2763–2774, doi:10.1063/1.858738.
[45] B. Al Zaitone, Oblate spheroidal droplet evaporation in an acoustic levitator, Int. J. Heat Mass Transf. 126 (2018) 164–172, doi:10.1016/j.ijheatmasstransfer.2018.06.029.
[46] C.P. Lee, A.V. Anilkumar, T.G. Wang, Static shape of an acoustically levitated drop with wave–drop interaction, Phys Fluids 6 (1994) 3554–3566, doi:10.1063/1.868414.
[47] W.J. Xie, B. Wei, Dynamics of acoustically levitated disk samples, Physical Review E 70 (2004) 046611, doi:10.1103/PhysRevE.70.046611.
[48] R. Tuckermann, S. Bauerecker, H.K. Cammenga, IR-thermography of evaporating acoustically levitated drops, Int. J. Thermophys. 26 (2005) 1583–1594, doi:10.1007/s10765-005-8105-6.
[49] N.O. and A. Administration, National Weather Service, 2019 (accessed August 29, 2019) https://www.weather.gov/epz/wxcalc_rh.
[50] Humidity calculator, (n.d.) accessed July 16, 2019 http://www.humcal.com/index.php.
[51] E. Bänsch, M. Götz, G. Michael, Numerical study of droplet evaporation in an acoustic levitator, Phys. Fluids (2018) 037103, doi:10.1063/1.5017936.
[52] T. Hellwig, Acoustic levitation as an analytical method for the investigation of multicomponent droplets, Universität Hamburg (2018).
[53] C. Verwey, M. Birouk, Experimental investigation of the effect of natural convection on the evaporation characteristics of small fuel droplets at moderately elevated temperature and pressure, Int. J. Heat Mass Transf. 118 (2018) 1046–1055, doi:10.1016/j.ijheatmasstransfer.2017.11.038.
[54] B. Al Zaitone, Evaporation of oblate spheroidal droplets: a theoretical analysis, Chem. Eng. Commun. 205 (2018) 110–121, doi:10.1080/00986445.2017.1374949.

[55] Z.L. Yan, W.J. Xie, B. Wei, Vortex flow in acoustically levitated drops, Phys. Lett. Sect. A 375 (2011) 3306–3309, doi:10.1016/j.physleta.2011.07.030.
[56] A. Saha, S. Basu, R. Kumar, Velocity and rotation measurements in acoustically levitated droplets, Phys. Lett. A 376 (2012) 3185–3191, doi:10.1016/j.physleta.2012.08.013.
[57] J.D. Smith, C.D. Cappa, W.S. Drisdell, R.C. Cohen, R.J. Saykally, Raman thermometry measurements of free evaporation from liquid water droplets, J. Am. Chem. Soc. 128 (2006) 12892–12898, doi:10.1021/ja063579v.
[58] R.J. Hopkins, C.R. Howle, J.P. Reid, Measuring temperature gradients in evaporating multicomponent alcohol/water droplets, Phys. Chem. Chem. Phys. 8 (2006) 2879, doi:10.1039/b600530f.
[59] P.A. Strizhak, R.S. Volkov, G. Castanet, F. Lemoine, O. Rybdylova, S.S. Sazhin, Heating and evaporation of suspended water droplets: experimental studies and modelling, Int. J. Heat Mass Transf. 127 (2018) 92–106, doi:10.1016/j.ijheatmasstransfer.2018.06.103.